



# Novel Engineered SARS-CoV-2 HR1 Trimer Exhibits Improved Potency and Broad-Spectrum Activity against SARS-CoV-2 and Its Variants

Wenwen Bi,<sup>a,b,c</sup> Guilin Chen,<sup>a,b,c</sup>  Bobo Dang<sup>a,b,c</sup>

<sup>a</sup>Key Laboratory of Structural Biology of Zhejiang Province, School of Life Sciences, Westlake University, Hangzhou, Zhejiang, China

<sup>b</sup>Center for Infectious Disease Research, Westlake Laboratory of Life Sciences and Biomedicine, Hangzhou, Zhejiang, China

<sup>c</sup>Institute of Biology, Westlake Institute for Advanced Study, Hangzhou, China

**ABSTRACT** The ongoing pandemic of COVID-19, caused by SARS-CoV-2, has substantially increased the risk to global public health. Multiple vaccines and neutralizing antibodies (nAbs) have been authorized for preventing and treating SARS-CoV-2 infection. However, the emergence and spread of the viral variants may limit the effectiveness of these vaccines and antibodies. Fusion inhibitors targeting the HR1 domain of the viral S protein have been shown to broadly inhibit SARS-CoV-2 and its variants. In theory, peptide inhibitors targeting the HR2 domain of the S protein should also be able to inhibit viral infection. However, previously reported HR1-derived peptide inhibitors targeting the HR2 domain exhibit poor inhibitory activities. Here, we engineered a novel HR1 trimer (HR1MFd) by conjugating the trimerization motif foldon to the C terminus of the HR1-derived peptide. HR1MFd showed significantly improved inhibitory activity against SARS-CoV-2, SARS-CoV-2 variants of concern (VOCs), SARS-CoV, and MERS-CoV. Mechanistically, HR1MFd possesses markedly increased  $\alpha$ -helicity, thermostability, higher HR2 domain binding affinity, and better inhibition of S protein-mediated cell-cell fusion compared to the HR1 peptide. Therefore, HR1MFd lays the foundation to develop HR1-based fusion inhibitors against SARS-CoV-2.

**IMPORTANCE** Peptides derived from the SARS-CoV-2 HR1 region are generally poor inhibitors. Here, we constructed a trimeric peptide HR1MFd by fusing the trimerization motif foldon to the C terminus of the HR1 peptide. HR1MFd was highly effective in blocking transductions by SARS-CoV-2, SARS-CoV-2 variants, SARS-CoV, and MERS-CoV pseudoviruses. In comparison with HR1M, HR1MFd adopted a much higher helical conformation, better thermostability, increased affinity to the viral HR2 domain, and better inhibition of S protein-mediated cell-cell fusion. Overall, HR1MFd provides the information to develop effective HR1-derived peptides as fusion inhibitors against SARS-CoV-2 and its variants.

**KEYWORDS** SARS-CoV-2, HR1, trimer, foldon, fusion inhibitor

Coronavirus disease 2019 (COVID-19) caused by severe acute respiratory syndrome coronavirus 2 (SARS-CoV-2) infection continues to be a major threat to global public health. Despite several COVID-19 vaccines and neutralizing antibodies having been approved for emergency use to prevent and treat SARS-CoV-2 infection, the emergence and spread of immune-escaping SARS-CoV-2 variants limit the effectiveness of these vaccines and neutralizing antibodies (1–3). Therefore, there remains an urgent need to develop highly effective and broad-spectrum antivirals that can combat SARS-CoV-2.

Similar to other coronaviruses (CoVs), SARS-CoV-2 infection requires the fusion of the viral membrane with the cell membrane, which is mediated by the viral spike (S) glycoprotein. The S protein is a trimeric class I fusion protein, composed of S1 and S2

**Editor** Tom Gallagher, Loyola University Chicago

**Copyright** © 2022 American Society for Microbiology. All Rights Reserved.

Address correspondence to Wenwen Bi, [biwenwen@westlake.edu.cn](mailto:biwenwen@westlake.edu.cn), or Bobo Dang, [dangbobo@westlake.edu.cn](mailto:dangbobo@westlake.edu.cn).

The authors declare no conflict of interest.

**Received** 3 May 2022

**Accepted** 2 June 2022

**Published** 23 June 2022

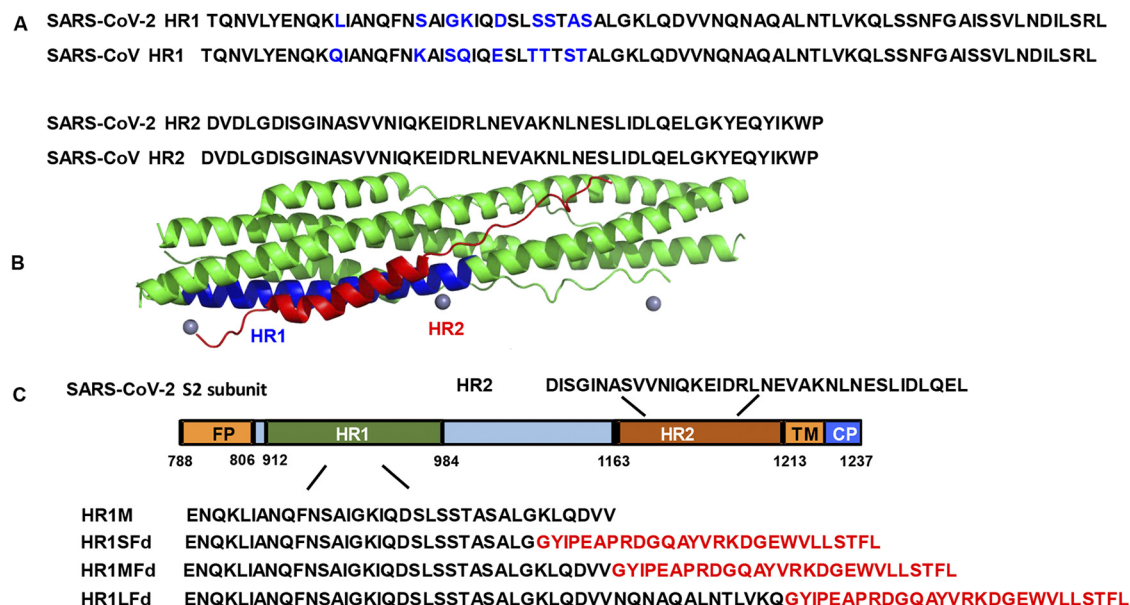


**FIG 1** Design of the HR1 trimers based on the sequence of the SARS-CoV-2 S protein S2 subunit. (A) Amino acid alignment of the HR1 and HR2 domains in SARS-CoV and SARS-CoV-2. (B) The structural basis of the interactions between HR1 and HR2 of SARS-CoV-2 (PDB: 6LXT). (C) Schematic representation of the SARS-CoV-2 S2 protein and sequences of the peptides. FP, fusion peptide region; HR1, heptad repeat 1 domain; HR2, heptad repeat 2 domain; TM, transmembrane region; CP, cytoplasm region. Foldon-conjugated HR1S, HR1M and HR1L proteins are shown in the diagram.

subunits (4, 5). The S1 subunit contains a receptor-binding domain (RBD) and an N-terminal domain (NTD), whereas the S2 subunit contains an N-terminal fusion peptide (FP), heptad repeat 1 (HR1), heptad repeat 2 (HR2), transmembrane domain (TM) and a cytoplasm domain (CP) (Fig. 1C) (6). During the fusion process, the S1 subunit binds to the cellular receptor angiotensin-converting enzyme 2 (ACE2) through RBD (7–9), then the HR1 and HR2 domains in the S2 subunit interact with each other to form a six-helix bundle (6-HB) (Fig. 1B), driving the fusion of target cell and viral membranes (10). Therefore, both S1 and S2 subunits can be targets for the development of SARS-CoV-2 entry inhibitors.

In previous studies, peptides derived from both the coronaviral HR1 and HR2 domains have been tested to block CoV infection, and HR2-derived peptides showed better inhibitory activity. Both Severe Acute Respiratory Syndrome Coronavirus (SARS-CoV) and the Middle East Respiratory Syndrome Coronavirus (MERS-CoV) HR2-derived peptides (CP1 and HR2P) exhibited potent inhibitory activity with half-maximal inhibitory concentration (IC<sub>50</sub>) in the micromolar range (11, 12). HCoV-OC43 HR2-derived peptide EK1 has been confirmed to be a pan-CoV fusion inhibitor against a wide variety of human CoVs (13). In comparison, CoVs HR1-derived peptides SARS-HR1P, MERS-HR1P, and 2019-nCoV-HR1P exhibited no inhibitory activity at any tested concentration (10–12), possibly because CoVs HR1-derived peptides may tend to aggregate, similar to HIV-1 N-terminal heptad repeat (NHR)-derived peptide inhibitors (14, 15). Therefore, the challenges remain in developing HR1-derived fusion inhibitors against different CoV strains.

Aiming to develop HR1-based fusion inhibitors, we fused the trimerization motif of T4 bacteriophage fibritin-foldon (Fd) to the C terminus of SARS-CoV-2 HR1-derived peptide to generate HR1 trimers (16, 17). Our results showed that these HR1-foldon peptides (HR1SFd, HR1MFd, and HR1LFd) indeed formed stable trimers. Among them, HR1MFd showed dramatically increased antiviral activity compared with the corresponding HR1 peptide. Mechanistically, the inhibitory activity of the Fd-conjugated HR1-derived peptide is strongly correlated with its stable helical conformation, high binding affinity with HR2 peptides, as well as its potent inhibition of S protein-mediated

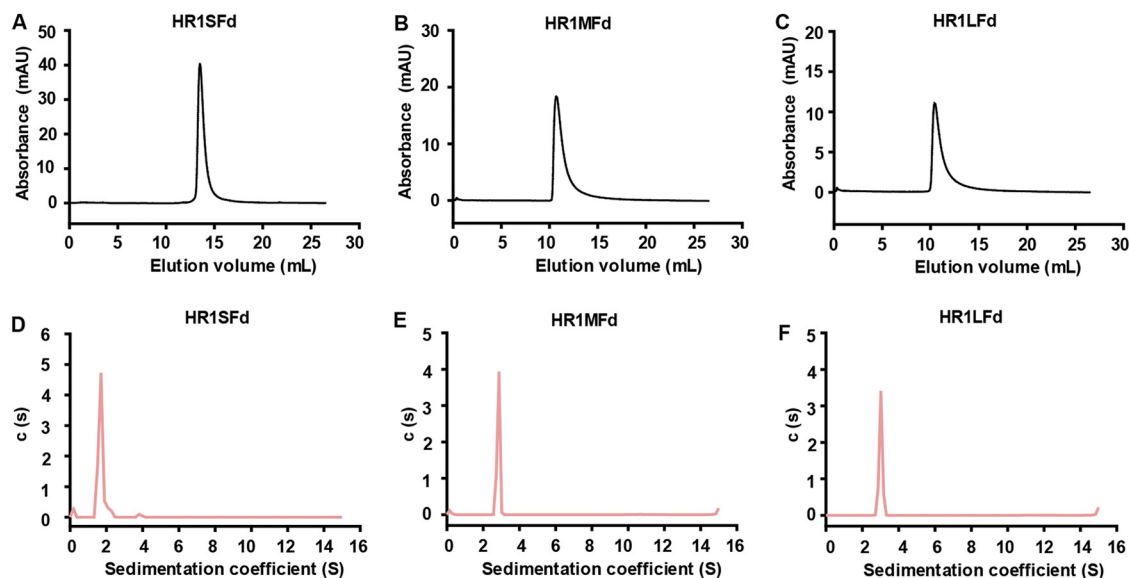


**FIG 2** SEC and AUC analysis of HR1SFd, HR1MFd and HR1LFd. Analytical SEC profiles of HR1SFd (A), HR1MFd (B), and HR1LFd (C) with Superdex 75 Increase 10/300 GL. The absorbance curve at 280 nm is shown. AUC analysis of HR1SFd (D), HR1MFd (E) and HR1LFd (F).

cell-cell fusion. Moreover, HR1MFd showed broad inhibitory activity against various SARS-CoV-2 pseudoviral mutants, two SARS-CoV-2 VOCs, SARS-CoV, and MERS-CoV. Further studies have shown that combining HR1MFd with T-ACE2 or mNb6 exhibited a synergistic inhibitory effect against SARS-CoV-2 pseudovirus transduction.

## RESULTS

**Design and biophysical characterization of HR1SFd, HR1MFd, and HR1LFd trimers.** SARS-CoV-2 has nine amino acid substitutions in the HR1 domain compared to SARS-CoV, whereas they share a fully identical HR2 domain (Fig. 1A). To develop HR1-derived viral inhibitors, we generated three different HR1 peptide trimers by fusing the foldon motif to the C terminus of HR1-derived short (HR1S), medium (HR1M), and long peptides (HR1L) (Fig. 1C). These peptides were expressed in *E. coli* and purified by nickel affinity chromatography and size exclusion chromatography (SEC). The SEC results indicated that HR1SFd, HR1MFd, and HR1LFd peptides have a molecular weight ranging from 20 to 30 kDa, suggesting the trimeric form (Fig. 2A to C). These peptides were further analyzed by analytical ultracentrifugation (AUC). The sedimentation coefficients of HR1SFd, HR1MFd, and HR1LFd were 1.71, 2.88, and 3.03 s and corresponded to molecular weights of 22.9 kDa, 24.7 kDa, and 29.0 kDa, which was close to the theoretical molecular weights of HR1SFd trimer (21.8 kDa), HR1MFd trimer (23.9 kDa), and HR1LFd trimer (28.1 kDa), respectively (Fig. 2D to F and Table 1). The friction coefficient ( $f/f_0$ ) in AUC provided the shape information of the analyzed protein. The friction coefficient of a hydrated protein is 1.2 to 1.4, whereas that of a moderately elongated protein is 1.6 to 1.9 (18). The  $f/f_0$  values of HR1SFd, HR1MFd, and HR1LFd trimers were extracted from the experimental data by using the SEDFIT program. As shown in Table 1, these recombinant peptides have a  $f/f_0$  value of 1.6 to 1.9, indicating the shapes of HR1SFd, HR1MFd and HR1LFd are moderately elongated.

**Conjugating the foldon motif to the C terminus of SARS-CoV-2 HR1-derived peptide enhanced the inhibitory activity.** We next evaluated the antiviral activities of HR1SFd, HR1MFd, and HR1LFd by using the SARS-CoV-2 pseudovirus transduction model in Huh-7 cells. As shown in Fig. 3A, SARS-CoV-2 HR1-derived peptide HR1M alone exhibited no significant inhibitory activity at concentrations up to 50  $\mu$ M, while HR1SFd, HR1MFd, and HR1LFd had dramatically improved inhibitory activity against SARS-CoV-2 pseudovirus transduction with  $IC_{50}$  of 4.6, 1.6, and 2.5  $\mu$ M, respectively.

**TABLE 1** Summary of AUC results of HR1SFd, HR1MFd, and HR1LFd

| Protein | Sedimentation coefficient (s) | Observed mol wt (kDa) | Calculated mol wt (kDa) | $f/f_0$ |
|---------|-------------------------------|-----------------------|-------------------------|---------|
| HR1SFd  | 1.71                          | 22.90                 | 21.80                   | 1.80    |
| HR1MFd  | 2.88                          | 24.70                 | 23.85                   | 1.63    |
| HR1LFd  | 3.03                          | 29.00                 | 28.12                   | 1.76    |

The previously studied HR2-derived peptide (HR2) was used as a positive-control in the same experiment and showed an  $IC_{50}$  of 14.8  $\mu$ M against SARS-CoV-2 pseudovirus transduction. HR1SFd, HR1MFd, and HR1LFd were also highly effective in inhibiting SRAS-CoV-2 pseudovirus transduction of human intestinal Caco-2 cells with  $IC_{50}$  of 4.8, 1.2, and 1.6  $\mu$ M, respectively (Fig. 3B). These results indicate that the addition of foldon to the C terminus of HR1 can indeed enhance its inhibitory activity.

To exclude the cytotoxic effect on the inhibitory activity, Huh-7 and Caco-2 cells were treated with a concentration gradient of HR1MFd for 48 h before evaluation of their viability with Cell Counting Kit-8 (CCK-8). As shown in Fig. S1, HR1MFd showed no significant cytotoxicity to Huh-7 and Caco-2 cells at concentrations up to 100  $\mu$ M, more than 62-fold higher than its  $IC_{50}$  for SARS-CoV-2 inhibition, suggesting that the inhibitory activity of peptides cannot be attributed to its cytotoxicity.

**Conjugating foldon to the C terminus of HR1M increased its  $\alpha$ -helicity and thermostability.** To explore the mechanism underlying the improved inhibitory activity of HR1MFd, we performed circular dichroism (CD) spectroscopy to evaluate the secondary conformation of HR1MFd. As shown in Fig. 4A, HR1M and Fd alone exhibited little  $\alpha$ -helicity. In contrast, HR1MFd displayed typical double negative peaks at 208 and 222 nm as  $\alpha$ -helical structures in the CD spectrum. These results indicated that the foldon motif in the HR1MFd facilitated the HR1M peptide folding into  $\alpha$ -helical conformation, mimicking the conformation of natural HR1 trimer in the fusion intermediate state during SARS-CoV-2 infection. The thermostability of HR1M and HR1MFd was also measured. The  $T_m$  value of HR1M could not be defined due to the lack of the secondary structures, while the HR1MFd had a  $T_m$  value of 51.9°C (Fig. 4B).

**Interactions between HR1MFd and SARS-CoV-2 HR2-derived peptide.** Previous studies showed that SARS-CoV-2 HR2-derived peptides could interact with HR1-derived peptides to prevent the entry of SARS-CoV-2 into target cells (10, 19). To explore if HR1MFd utilizes a similar mechanism against SARS-CoV-2 infection, we first characterized the secondary structure of the complex of HR1MFd with HR2 peptide by CD. HR1MFd and HR2 were incubated at an equal concentration at 37°C for 30 min, and the CD spectrum of the mixture was measured. The result showed that although both

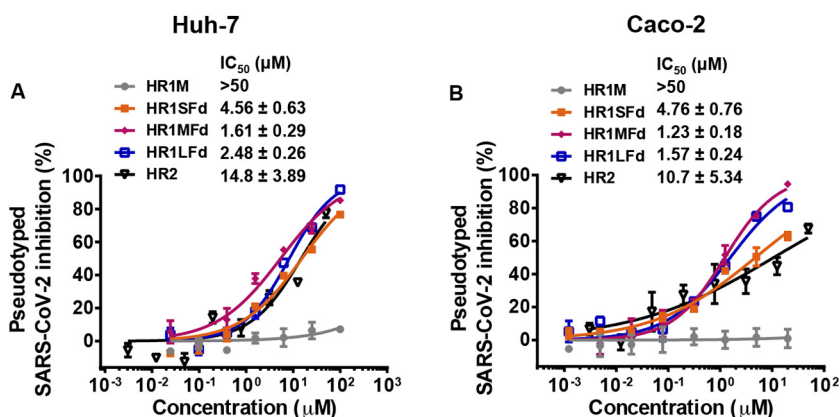


**FIG 3** Inhibitory activity of foldon-conjugated HR1-derived peptides against SARS-CoV-2 pseudovirus transduction. The inhibitory activity of HR1M, HR1SFd, HR1MFd, HR1LFd, or HR2 against SARS-CoV-2 pseudovirus in Huh-7 (A) and Caco-2 cells (B). Each sample was tested in triplicate and the data are presented as mean  $\pm$  SEM.

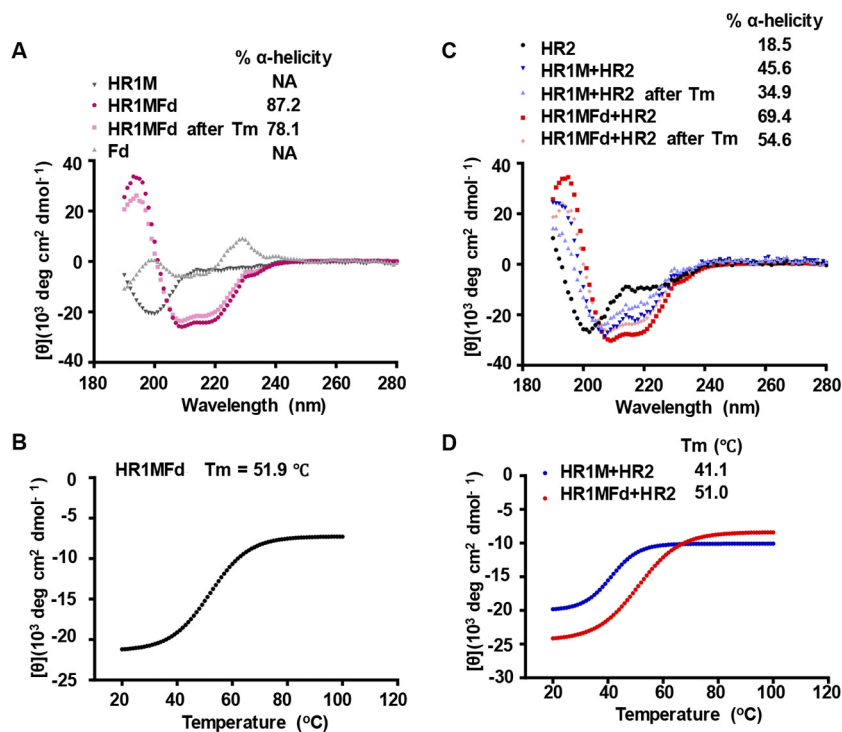


**FIG 4** Secondary structure and thermostability of HR1MFd determined by CD spectroscopy. The  $\alpha$ -helicity and thermostability of HR1MFd alone (A and B) or in complexes with SARS-CoV-2 HR2 peptide (C and D) were detected with a final concentration of each peptide at 20  $\mu$ M. The experiments were performed twice, and representative data are shown. NA, not available.

HR1M and HR1MFd interacted with HR2 peptides to form complexes with the characteristic  $\alpha$ -helical structure, HR1MFd exhibited a higher  $\alpha$ -helical structure with HR2 than HR1M did, while HR2 exhibited a low  $\alpha$ -helical structure by itself (<20%) (Fig. 4C). We also measured the thermostability of the complex formed between HR2 and HR1M or HR1MFd. As shown in Fig. 4D, the  $T_m$  value of the HR2 and HR1MFd complex (51°C) was higher than that of the HR2 and HR1M complex (41°C).

We subsequently compared the binding affinity of HR2 with HR1M and HR1MFd by using biolayer interferometry (BLI). As shown in Fig. 5 and Table 2, HR1MFd could bind to HR2 peptide in a dose-dependent manner ( $K_D = 1.7 \mu$ M), while HR1M could not.

Taken together, these results suggested that HR1MFd showed enhanced binding affinity to SARS-CoV-2 HR2 compared with HR1M, which probably was the reason for the improved SARS-CoV-2 inhibitory activity.

**HR1MFd could effectively inhibit SARS-CoV-2 S protein-mediated cell-cell fusion.** We used an established S protein-mediated cell-cell fusion assay to explore the possible mechanism where HR1MFd inhibits SARS-CoV-2 infection by blocking SARS-

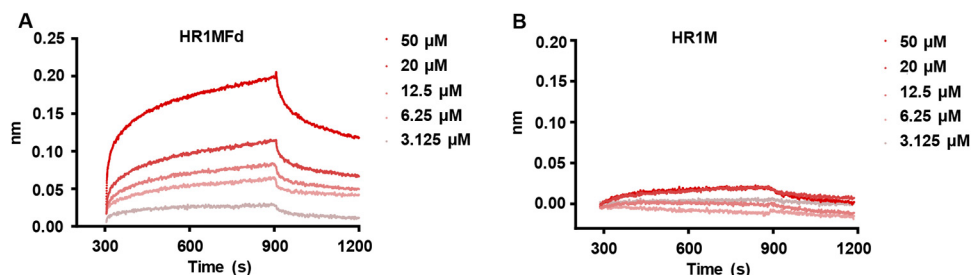


**FIG 5** Binding affinity measurement using BLI. (A) The binding affinity of HR1MFd to HR2 was determined by BLI. (B) The binding affinity of HR1M to HR2 was determined by BLI. The fitting curve was analyzed by ForteBio Data Analysis 12.0 software.

**TABLE 2** Binding affinity of HR1MFd or HR1M to SARS-CoV-2 HR2 peptide, as determined by BLI<sup>a</sup>

| Protein | K <sub>D</sub> (M) | K <sub>on</sub> (1/Ms) | K <sub>off</sub> (1/s) |
|---------|--------------------|------------------------|------------------------|
| HR1M    | –                  | –                      | –                      |
| HR1MFd  | 1.71E–06           | 8.13E+02               | 1.39E–03               |

<sup>a</sup>The data were presented as mean values. –, not detected.

CoV-2 S protein-mediated fusion (20). In the assay, 293T cells coexpressing SARS-CoV-2 D614G S protein and EGFP (293T/EGFP/S) were used as the effector cells, and ACE2 expressing Caco-2 or Huh-7 cells were used as the target cells. As expected, after coculture of the effector and target cells, effector cells are effectively fused with Caco-2 or Huh-7 cells. As shown in Fig. 6A, the fused cells exhibited larger sizes than normal cells and contained multiple nuclei. However, 293T cells expressing EGFP only (293T/EGFP) could not fuse with either Caco-2 or Huh-7 cells (Fig. S2). Considering that HR1 and HR2 play an important role in mediating the fusion between viral and target cell membranes, we speculated that HR1MFd may prevent the fusion between SARS-CoV-2 and target cells. We thus assessed the inhibitory activity of HR1MFd on SARS-CoV-2 D614G S protein-mediated cell-cell fusion. As shown in Fig. 6B and D, HR1MFd could effectively inhibit SARS-CoV-2 D614G S protein-mediated cell-cell fusion between 293T/EGFP/S and Huh-7 cells in a dose-dependent manner with an IC<sub>50</sub> of 1.1 μM, while neither HR1M nor Fd (IC<sub>50</sub> >20 μM) can inhibit such cell-cell fusion. HR1MFd could also block D614G S protein-mediated cell-cell fusion between 293T/EGFP/S and Caco-2 cells with an IC<sub>50</sub> of 0.74 μM (Fig. 6C). The previously studied HR2 peptide was used as a positive control and showed slightly less efficiency in inhibiting 293T/EGFP/S cells fusion with Huh-7 (IC<sub>50</sub> = 1.76 μM) and Caco-2 cells (IC<sub>50</sub> = 1.14 μM).

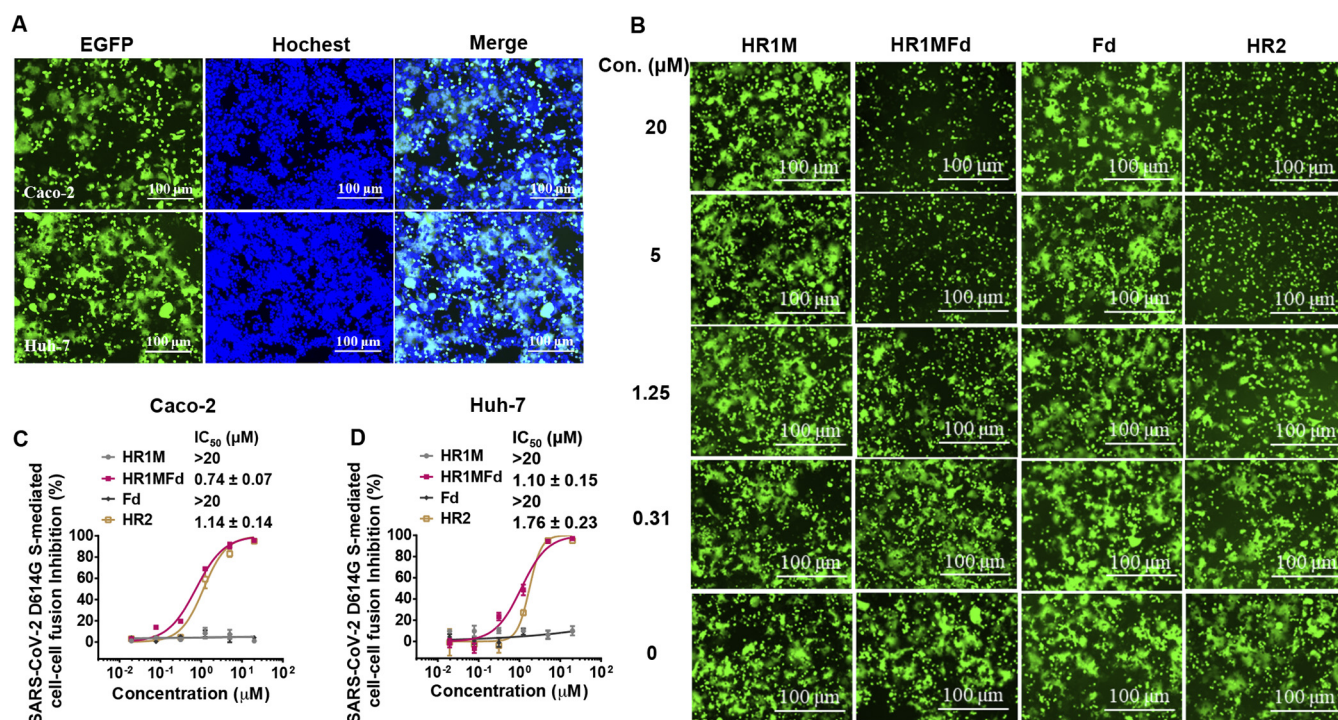


**FIG 6** Inhibitory activity of HR1MFd against SARS-CoV-2 D614G S protein-mediated cell-cell fusion. (A) Representative images of D614G S protein-mediated cell-cell fusion between 293T/EGFP/S effector cells and Caco-2 or Huh-7 target cells. Scale bars, 100 μm. (B) Images of D614G S protein-mediated cell-cell fusion in the presence of HR1M, HR1MFd, Fd, or HR2 at indicated concentrations after coculture of 293T/EGFP/S effector cells and Huh-7 target cells. Scale bars, 100 μm. The inhibitory activity of HR1M, HR1MFd, Fd, or HR2 against D614G S protein-mediated cell-cell fusion between 293T/EGFP/S effector cells and Caco-2 cells (C) or Huh-7 cells (D). Samples were tested twice, and the experiment was performed twice. Data from a representative experiment are presented as mean ± SEM.

**TABLE 3** Inhibitory activity of HR1M, Fd, and HR1MFd against SARS-CoV-2 variants pseudovirus transduction<sup>a</sup>

| SARS-CoV-2 variants | IC <sub>50</sub> ± SD (μM) |     |             |
|---------------------|----------------------------|-----|-------------|
|                     | HR1M                       | Fd  | HR1MFd      |
| E406W               | >50                        | >50 | 3.16 ± 0.75 |
| D614G               | >50                        | >50 | 3.03 ± 0.52 |
| N501Y               | >50                        | >50 | 1.12 ± 0.22 |
| N439K               | >50                        | >50 | 2.03 ± 0.30 |
| K417N               | >50                        | >50 | 2.02 ± 0.25 |
| A701V               | >50                        | >50 | 3.15 ± 1.46 |
| E484K               | >50                        | >50 | 1.48 ± 0.43 |
| K417N/N501Y         | >50                        | >50 | 1.66 ± 0.62 |
| E484K/N501Y         | >50                        | >50 | 1.37 ± 0.31 |
| N439K/N501Y         | >50                        | >50 | 2.41 ± 0.84 |
| K417N/E484K/N501Y   | >50                        | >50 | 1.13 ± 0.25 |
| Average             | >50                        | >50 | 2.05        |

<sup>a</sup>Each sample was tested in triplicate and the data were presented as mean ± SEM. When the average was calculated, the value of IC<sub>50</sub> >50 μM was tested as 50 μM.

**HR1MFd exhibited broad and potent inhibitory activity against different SARS-CoV-2 variants, SARS-CoV, and MERS-CoV.** To test whether HR1MFd can broadly inhibit different coronavirus strains, we evaluated the antiviral activities of HR1M, Fd, and HR1MFd against pseudotyped SARS-CoV-2 variants with single or multiple key mutations in the S protein. As shown in Table 3, HR1M and Fd were unable to inhibit any of the pseudotyped SARS-CoV-2 variants at concentrations up to 50 μM, while HR1MFd could efficiently suppress the transduction of 11 pseudotyped SARS-CoV-2 variants with an average IC<sub>50</sub> of 2.05 μM, about 24-fold more potent than HR1M. These results suggested that HR1MFd could effectively inhibit SARS-CoV-2 variants with mutations in the S protein.

We then assessed the inhibitory activity of HR1MFd against pseudotyped SARS-CoV-2 VOCs, including Alpha (B.1.1.7) and Omicron (B.1.1.529). As shown in Fig. 7A and B, we found that HR1MFd was effective in inhibiting pseudotyped Alpha and Omicron variants with IC<sub>50</sub> of 2.35 and 1.06 μM, respectively, showing higher potency than that of HR1M (IC<sub>50</sub> >50 μM). Meanwhile, HR1MFd could also effectively block the transduction of the pseudotyped SARS-CoV and MERS-CoV with IC<sub>50</sub> of 2.13 and 2.86 μM, which was also more effective than HR1M (IC<sub>50</sub> >50 μM) (Fig. 7C and D). The previously studied HR2 peptide used as a positive control could also inhibit SARS-CoV-2 Alpha, Omicron, SARS-CoV, and MERS-CoV transductions with IC<sub>50</sub> ranging from 5.27 to 10.9 μM. These results suggest that HR1MFd is effective against SARS-CoV-2 variants, SARS-CoV and MERS-CoV.

**Combining HR1MFd with T-ACE2 or mNb6 resulted in potent synergistic anti-SARS-CoV-2 activity.** Subsequently, we evaluated the combination of SARS-CoV-2 HR2-targeting inhibitor HR1MFd and RBD-targeting protein T-ACE2 for potential synergism against SARS-CoV-2 pseudovirus transduction (21). The inhibition of SARS-CoV-2 by T-ACE2, HR1MFd, or T-ACE2/HR1MFd mixture was determined by using a pseudovirus system, the combination index (CI) and dose-reductions were analyzed by using CalcuSyn software kindly provided by T.C. Chou (22, 23). As shown in Fig. S3A and Table S1, a combination of HR1MFd and T-ACE2 showed a synergistic effect against SARS-CoV-2 pseudovirus transduction with a CI of 0.11, with dose reductions of 5-fold for HR1MFd and 2-fold for T-ACE2, respectively. We next tested the combination of HR1MFd with mNb6 nanobody that was reported to bind to the closed conformation of S protein (24). We found that the combination of HR1MFd with mNb6 exhibited stronger synergy (CI = 0.05), with the dose reductions being 10- and 18-fold of HR1MFd and mNb6, respectively (Fig. S3B and Table S1). To better illustrate these results, we further presented the concentration of 50% inhibition (IC<sub>50</sub>) from the data in Fig. S3A and B in an isobologram format. As shown in Fig. S3C and D, the

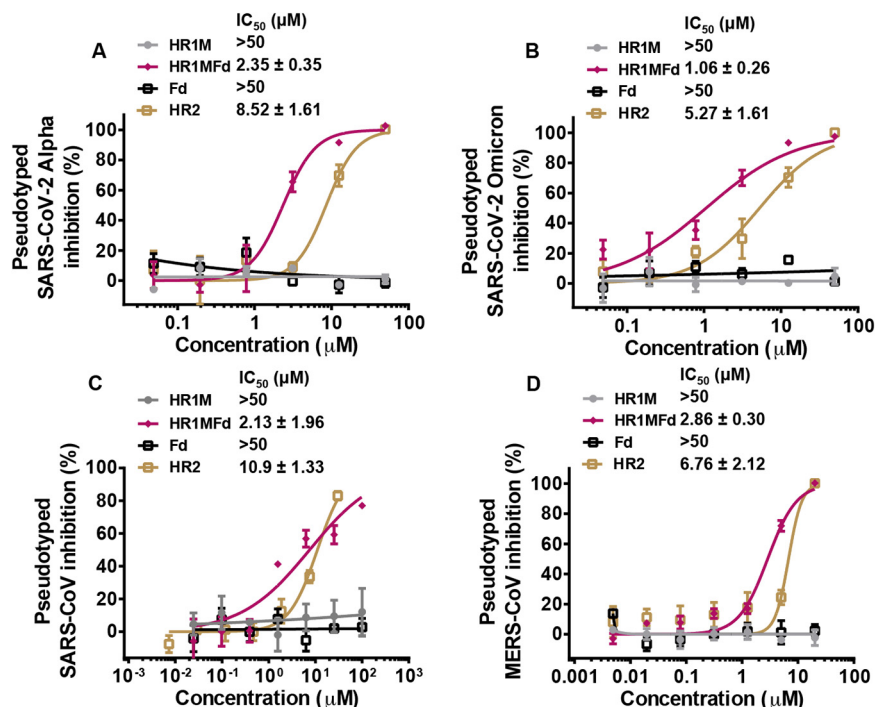


**FIG 7** Inhibitory activity of HR1MFd against SARS-CoV-2 VOCs, SARS-CoV, and MERS-CoV pseudovirus transduction. The inhibitory activity of HR1M, Fd, HR1MFd, or HR2 against SARS-CoV-2 Alpha (A) and Omicron (B) pseudovirus transduction in Caco-2 cells. (C) The effect of HR1M, Fd, HR1MFd, or HR2 on the transduction of SARS-CoV pseudovirus in Caco-2 cells. (D) The effect of HR1M, Fd, HR1MFd, or HR2 on the transduction of MERS-CoV pseudovirus in Caco-2 cells. Each sample was tested in triplicate and the data are presented as mean ± SEM.

experimental data points corresponding to the IC<sub>50</sub> needed for the combination of both HR1MFd/T-ACE2 and HR1MFd/mNb6 fell on the lower left of the additivity line, indicating that both HR1MFd/T-ACE2 and HR1MFd/mNb6 combination exhibited synergistic inhibitory effect. These results suggested that HR1MFd and neutralizing proteins or antibodies could be used in combination for the synergistic inhibition of SARS-CoV-2 infection.

**DISCUSSION**

Although the application of SARS-CoV-2 vaccines has shown significant efficacy in the reduction of hospitalization and deaths, several SARS-CoV-2 variants, especially the Omicron variant, can evade vaccine-induced immunity and neutralizing antibodies extensively (25, 26). Therefore, it is an urgent need to develop potent and broad-spectrum antiviral inhibitors against SARS-CoV-2 and its variants. One promising strategy is to target the conserved HR1 or HR2 domains of the viral S protein. Indeed, unmodified, or cholesterol-modified HR2-derived peptides targeting the viral HR1 region have previously been shown to be effective inhibitors (27, 28). Theoretically, HR1-derived inhibitors (targeting HR2 region) should also have broad and potent anti-coronavirus activity. However, previously studied CoVs HR1-derived peptides are poor inhibitors against CoVs infection.

To design potent HR1-derived inhibitors, we developed a novel strategy by fusing the T4 bacteriophage trimerization domain foldon to the C terminus of SARS-CoV-2 HR1-derived peptides to allow HR1 peptides to form trimers (Fig. 1C). As expected, the engineered HR1SFd, HR1MFd, and HR1LFd peptides exhibited trimeric conformation and had significantly better anti-SARS-CoV-2 activity than HR1 itself. Due to the conserved SARS-CoV-2 HR2 domain, we also found that HR1MFd could effectively block the transduction of several other pseudotyped SARS-CoV-2 variants, including

the currently dominant Omicron variant (Fig. 7A and B). Meanwhile, HR1MFd is also effective in inhibiting the transduction of SARS-CoV and MERS-CoV pseudoviruses.

In summary, the addition of foldon to the C terminus of HR1M, designated HR1MFd, dramatically stabilized the  $\alpha$ -helical conformation of HR1M, contributing to the potent and broad inhibitory activity against CoVs, including the currently dominant SARS-CoV-2 variants, SARS-CoV and MERS-CoV. In addition, a combination of HR1MFd with T-ACE2 or mNhb6 exhibited a synergistic inhibitory effect, which could potentially help reduce the dose of antibodies as well as avoid the escape of novel viral mutants.

## MATERIALS AND METHODS

**Peptides.** Peptides (Fig. 1A) were synthesized on the H-Rink-Amid-ChemMatrix resin using a standard solid-phase 9-fluorenylmethoxycarbonyl (Fmoc). All peptides were acetylated at the N terminus before resin cleavage and characterized with mass spectrometry. The purities of peptides were more than 90%, as determined by reversed-phase high-pressure liquid chromatography (HPLC). The peptides were dissolved in dimethyl sulfoxide (DMSO) or PBS.

**Plasmids and cells.** The S protein-expressing plasmids pcDNA3.1-SARS-CoV-S, pcDNA3.1-SARS-CoV-2-S, and the luciferase-expressing plasmid pNL4-3.Luc.RE was kindly provided by Shibo Jiang and Lu Lu at Shanghai Medical College of Fudan University. The SARS-CoV-2 S protein mutants expressing plasmids were generated by using overlap PCR. SARS-CoV-2 Alpha and Omicron S protein-expressing plasmids were purchased from Genewiz, Suzhou, China. The plasmid pcDNA3.1 encoding the EGFP and SARS-CoV-2 D614G S protein (pcDNA3.1-EGFP-P2A-SARS-CoV-2 D614G S) or encoding the EGFP protein (pcDNA3.1-EGFP) were kindly provided by Mingqi Xie at Westlake University. The cell lines, including 293T, Caco-2, and Huh-7 were also kindly provided by Shibo Jiang and Lu Lu, and cultured in DMEM with 10% fetal bovine serum (FBS).

**Expression and purification of the engineered HR1 peptides.** HR1SFd, HR1MFd, and HR1LFd peptides were obtained by fusing the T4 bacteriophage fibrin-derived foldon peptide directly to the C terminus of HR1-derived short (HR1S), medium (HR1M) and long (HR1L) peptides, respectively (Fig. 1C). The genes of HR1SFd, HR1MFd, and HR1LFd were synthesized and cloned into a pET28a vector by Genewiz, Suzhou, China.

pET28a-HR1SFd, pET28a-HR1MFd, and pET28a-HR1LFd plasmids were transformed into *E. coli* BL21 (DE3), respectively. The cells were incubated at 37°C in an LB medium until the OD<sub>600</sub> reached 0.8. The peptides were induced with 0.5 mM isopropyl 1-thio- $\beta$ -D-galactopyranoside for 6 h at 37°C. Then the cells were harvested, sonicated in PBS with 1% Triton and centrifuged at 1,200 g for 10 min. The supernatant was loaded into Ni-NTA beads (Smart-Lifesciences, catalog no. SA004100) and washed with 10 mM imidazole in PBS. Peptides were then eluted with elution buffer (250 mM imidazole in PBS). The peak fractions were collected and concentrated with a 10 kDa ultrafiltration tube (Millipore, Germany). The peptides were then analyzed by size exclusion chromatography (Superdex 75 Increase 10/300 GL, GE Healthcare) in the CH<sub>3</sub>COONa/CH<sub>3</sub>COOH buffer (pH 6.0).

**Analytical ultracentrifugation (AUC) molecular weight determination.** AUC experiments were performed on the analytical ultracentrifuge (Beckman Coulter, Fullerton, CA) equipped with an eight-cell An-50 Ti rotor. The peptide samples were centrifuged in 100 mM CH<sub>3</sub>COONa/CH<sub>3</sub>COOH (pH 6.0). The mixture of 20  $\mu$ M HR1MFd and HR2 was centrifuged in PBS (pH 7.4). The sample (385  $\mu$ L) and corresponding buffer (400  $\mu$ L) were loaded pairwise into the double sector quartz cell and run at 38,000 rpm at 20°C. Data were collected at the wavelength of 280 nm in a continuous scan mode with scanning spaces of 20 s. Sedimentation coefficient distribution,  $c(s)$ , and molar mass distribution,  $c(M)$ , were calculated by using the program SEDFIT. The partial specific volume, buffer density, and viscosity were calculated by using SEDNTERP.

**Inhibition of the pseudotyped virus transduction.** SARS-CoV-2 and its variants were generated, as described previously (27, 29). Briefly, 293T cells were cotransfected with the plasmid encoding the S protein of SARS-CoV-2 or its variants, and the luciferase-expressing HIV-1 genome plasmid by using Vigofect reagent (Vigorous Biotech, Beijing, China). The supernatants were collected at 48 h posttransfection, centrifuged at 3,000 g for 10 min, and stored at -80°C for single-cycle infection. The antiviral activities of the peptides were determined by using Huh-7 and Caco-2 cells ( $10^4$ /well) transduced by SARS-CoV-2 pseudovirus. The supernatants were replaced with fresh DMEM with 10% FBS at 12 h postinfection and the cells were cultured for an additional 48 h at 37°C. The cells were lysed, and the luciferase activity was measured by using a luciferase kit (Promega, Madison, WI, USA) on a microplate reader (Thermo, Variokan LUX). All inhibition curves of best fit were drawn using GraphPad Prism.

**Circular dichroism (CD) spectroscopy.** CD spectroscopy was conducted, as previously described (29). Briefly, the HR2 peptide was incubated at equal molar concentration with HR1MFd at 37°C for 30 min. Two peptides alone were also used as control. The final concentration of each peptide was 20  $\mu$ M in phosphate buffer (PB, pH 7.2). The CD spectra were measured on a Chirascan Spectrometer (model Chirascan V100; Applied Photophysics Ltd., UK), using a 1-nm bandwidth with a 1-nm step resolution from 190 to 280 nm at room temperature. The spectra were corrected by subtraction of a solvent blank (PB). The  $\alpha$ -helical content was calculated from the CD signal by dividing the mean residue ellipticity  $[\theta]$  at 222 nm by the value expected for 100% helix formation ( $-33,000 \text{ deg cm}^2 \text{ dmol}^{-1}$ ) (30). Melting temperature was determined by monitoring the change in ellipticity  $[\theta]$  at 222 nm at increasing temperature (20 to 100°C), using a temperature controller. The temperature was increased at a rate of 5°C/min; data were acquired at a 1-nm bandwidth at 222 nm at a frequency of 0.25 Hz. The melting

curve was smoothed, and the midpoint of the thermal unfolding transition ( $T_m$ ) value was taken as the maximum of the derivative  $d[\theta]_{222}/dt$ .

**Binding affinity determination using bio-layer interferometry (BLI).** HR2 peptide was biotinylated at a theoretical 1:3 molar ratio with EZ-Link NHS-PEG12-Biotin (Thermo Fisher Scientific) according to the manufacturer's instructions. The unreacted biotin was removed by ultrafiltration with an Amicon column (3 kDa MWCO, Millipore). For kinetic analysis, HR2 was captured on the streptavidin biosensors. Biotinylated HR2 peptide was diluted to 10  $\mu\text{g}/\text{mL}$  in a dilution buffer (PBS with 0.02% Tween 20 and 0.1% BSA). The background signal was measured using a reference sensor with HR2 peptide loading but no inhibitor binding and was subtracted from the corresponding inhibitor binding sensor. Curve fitting was performed by using the ForteBio data analysis software. Mean  $k_{\text{on}}$ ,  $k_{\text{off}}$ , and  $K_D$  values were determined by averaging all binding curves that matched the theoretical fit with an  $R^2$  value of 0.96.

**Inhibition of SARS-CoV-2 D614G S-mediated cell-cell fusion.** The establishment and detection of cell-cell fusion assay by using a method similar to that for determining HIV-1 Env-mediated cell-cell fusion (29). In brief, 293T cells were transfected with the plasmids pcDNA3.1 encoding the EGFP and SARS-CoV-2 D614G S protein (293T/EGFP/S protein) or encoding the EGFP protein (293T/EGFP) and used as the effector cells. Huh-7 cells or Caco-2 cells were used as the target cells. For SARS-CoV-2 D614G S-mediated cell-cell fusion assays, target cells were cultured at 37°C overnight, then 293T/EGFP/S effector cells were added in the presence or absence of the tested inhibitors at graded indicated concentrations. After coculture at 37°C for 5 h, three fields were randomly selected in each well to count the number of fused and unfused cells under an inverted fluorescence microscope (ZEISS, Germany).

**Detection of the inhibitory activity of HR1MFd with the neutralizing antibody or protein.** The synergistic effect of HR1MFd with neutralizing antibody mNb6 or protein T-ACE2 against SARS-CoV-2 pseudovirus was tested as described above. T-ACE2 or mNb6 were mixed with HR1MFd at the indicated molar concentration ratio, whereas mNb6 alone, T-ACE2 alone, and HR1MFd alone were included as controls. The samples were serially diluted and incubated with virus at 37°C for 30 min, then the mixture was added to the cells. The data were analyzed for synergistic effect by calculating the combination index (CI) with the CalcuSyn program (23). CI values of  $<1$  and  $>1$  indicate synergy and antagonism, respectively (22). The fold of dose reduction was indicated by the ratio of concentrations of inhibitors tested in combination over alone.

**Cell viability assay.** The potential cytotoxicity of peptides on Huh-7 and Caco-2 cells was measured by using the Cell Counting Kit-8 (CCK-8, Dojindo) according to the manufacturer's instructions. Briefly, 100  $\mu\text{L}$  of inhibitors at indicated concentrations were added to equal volumes of cells ( $10^4$  cells/well) in a 96-well plate. Cell viability was evaluated by using the CCK-8 after incubation at 37°C for 2 days. After incubation with the CCK-8 reagents at 37°C for another 2 h, the absorbance at 450 nm was measured with an ELISA reader, and the percentage of cytotoxicity was calculated.

## SUPPLEMENTAL MATERIAL

Supplemental material is available online only.

**SUPPLEMENTAL FILE 1**, PDF file, 2 MB.

## ACKNOWLEDGMENTS

We thank Shibo Jiang and Lu Lu at Shanghai Medical College of Fudan University, for providing the plasmids of pcDNA3.1-SARS-CoV-S, pcDNA3.1-SARS-CoV-2-S, and pNL4-3.Luc.RE, as well as the cell lines, including 293T, Caco-2, and Huh-7. We also want to thank the Mass Spectrometry and Metabolomics Core Facility, and the Protein Characterization and Crystallography Facility at the Center for Biomedical Research Core Facilities of Westlake University for sample analysis.

This work was supported by the Westlake Education Foundation and Tencent Foundation, the Zhejiang Key R&D Program of Zhejiang Province (no. 2021C03040), the Natural Science Foundation of China (no. 22077104; 32120103013), and the fellowship of the China Postdoctoral Science Foundation (file no. 2021M692880 to W.B.). The funders had no role in study design, data collection, interpretation, or the decision to submit the work for publication.

We declare no conflict of interest.

## REFERENCES

- Wang P, Nair MS, Liu L, Iketani S, Luo Y, Guo Y, Wang M, Yu J, Zhang B, Kwong PD, Graham BS, Mascola JR, Chang JY, Yin MT, Sobieszczyk M, Kyratsous CA, Shapiro L, Sheng Z, Huang Y, Ho DD. 2021. Antibody resistance of SARS-CoV-2 variants B.1.351 and B.1.1.7. *Nature* 593:130–135. <https://doi.org/10.1038/s41586-021-03398-2>.
- Madhi SA, Baillie V, Cutland CL, Voysey M, Koen AL, Fairlie L, Padayachee SD, Dheda K, Barnabas SL, Bhorat QE, Briner C, Kwatra G, Ahmed K, Aley P, Bhikha S, Bhiman JN, Bhorat AE, Du Plessis J, Esmail A, Groenewald M, Horne E, Hwa SH, Jose A, Lambe T, Laubscher M, Malahleha M, Masenya M, Masilela M, McKenzie S, Molapo K, Moultrie A, Oelofse S, Patel F, Pillay S, Rhead S, Rodel H, Rossouw L, Taoushanis C, Tegally H, Thombayil A, van Eck S, Wibmer CK, Durham NM, Kelly EJ, Villafana TL, Gilbert S, Pollard AJ, de Oliveira T, Moore PL, Sigal A, Izu A, Group N-S, Wits VCG, Wits-VIDA COVID Group. 2021. Efficacy of the ChAdOx1 nCoV-19 Covid-19 vaccine against the B.1.351 variant. *N Engl J Med* 384:1885–1898. <https://doi.org/10.1056/NEJMoa2102214>.

3. Weisblum Y, Schmidt F, Zhang F, DaSilva J, Poston D, Lorenzi JC, Muecksch F, Rutkowska M, Hoffmann HH, Michailidis E, Gaebler C, Agudelo M, Cho A, Wang Z, Gazumyan A, Cipolla M, Luchsinger L, Hillyer CD, Caskey M, Robbiani DF, Rice CM, Nussenzweig MC, Hatzioannou T, Bieniasz PD. 2020. Escape from neutralizing antibodies by SARS-CoV-2 spike protein variants. *Elife* 9:e61312. <https://doi.org/10.7554/eLife.61312>.
4. Zhou P, Yang XL, Wang XG, Hu B, Zhang L, Zhang W, Si HR, Zhu Y, Li B, Huang CL, Chen HD, Chen J, Luo Y, Guo H, Jiang RD, Liu MQ, Chen Y, Shen XR, Wang X, Zheng XS, Zhao K, Chen QJ, Deng F, Liu LL, Yan B, Zhan FX, Wang YY, Xiao GF, Shi ZL. 2020. A pneumonia outbreak associated with a new coronavirus of probable bat origin. *Nature* 579:270–273. <https://doi.org/10.1038/s41586-020-2012-7>.
5. Wrapp D, Wang N, Corbett KS, Goldsmith JA, Hsieh CL, Abiona O, Graham BS, McLellan JS. 2020. Cryo-EM structure of the 2019-nCoV spike in the prefusion conformation. *Science* 367:1260–1263. <https://doi.org/10.1126/science.abb2507>.
6. Walls AC, Park YJ, Tortorici MA, Wall A, McGuire AT, Veesler D. 2020. Structure, function, and antigenicity of the SARS-CoV-2 spike glycoprotein. *Cell* 183:1735. <https://doi.org/10.1016/j.cell.2020.11.032>.
7. Hoffmann M, Kleine-Weber H, Schroeder S, Kruger N, Herrler T, Erichsen S, Schiergens TS, Herrler G, Wu NH, Nitsche A, Muller MA, Drosten C, Pohlmann S. 2020. SARS-CoV-2 cell entry depends on ACE2 and TMPRSS2 and is blocked by a clinically proven protease inhibitor. *Cell* 181:271–280.e278. <https://doi.org/10.1016/j.cell.2020.02.052>.
8. Wang Q, Zhang Y, Wu L, Niu S, Song C, Zhang Z, Lu G, Qiao C, Hu Y, Yuen KY, Wang Q, Zhou H, Yan J, Qi J. 2020. Structural and functional basis of SARS-CoV-2 entry by using human ACE2. *Cell* 181:894–904.e899. <https://doi.org/10.1016/j.cell.2020.03.045>.
9. Shang J, Ye G, Shi K, Wan Y, Luo C, Aihara H, Geng Q, Auerbach A, Li F. 2020. Structural basis of receptor recognition by SARS-CoV-2. *Nature* 581:221–224. <https://doi.org/10.1038/s41586-020-2179-y>.
10. Xia S, Zhu Y, Liu M, Lan Q, Xu W, Wu Y, Ying T, Liu S, Shi Z, Jiang S, Lu L. 2020. Fusion mechanism of 2019-nCoV and fusion inhibitors targeting HR1 domain in spike protein. *Cell Mol Immunol* 17:765–767. <https://doi.org/10.1038/s41423-020-0374-2>.
11. Liu S, Xiao G, Chen Y, He Y, Niu J, Escalante CR, Xiong H, Farmer J, Debnath AK, Tien P, Jiang S. 2004. Interaction between heptad repeat 1 and 2 regions in spike protein of SARS-associated coronavirus: implications for virus fusogenic mechanism and identification of fusion inhibitors. *Lancet* 363:938–947. [https://doi.org/10.1016/S0140-6736\(04\)15788-7](https://doi.org/10.1016/S0140-6736(04)15788-7).
12. Lu L, Liu Q, Zhu Y, Chan KH, Qin L, Li Y, Wang Q, Chan JF, Du L, Yu F, Ma C, Ye S, Yuen KY, Zhang R, Jiang S. 2014. Structure-based discovery of Middle East respiratory syndrome coronavirus fusion inhibitor. *Nat Commun* 5:3067. <https://doi.org/10.1038/ncomms4067>.
13. Xia S, Yan L, Xu W, Agrawal AS, Algaissi A, Tseng CK, Wang Q, Du L, Tan W, Wilson IA, Jiang S, Yang B, Lu L. 2019. A pan-coronavirus fusion inhibitor targeting the HR1 domain of human coronavirus spike. *Sci Adv* 5:eaav4580. <https://doi.org/10.1126/sciadv.aav4580>.
14. Root MJ, Kay MS, Kim PS. 2001. Protein design of an HIV-1 entry inhibitor. *Science* 291:884–888. <https://doi.org/10.1126/science.1057453>.
15. Eckert DM, Kim PS. 2001. Design of potent inhibitors of HIV-1 entry from the gp41 N-peptide region. *Proc Natl Acad Sci U S A* 98:11187–11192. <https://doi.org/10.1073/pnas.201392898>.
16. Gao G, Wiczorek L, Peachman KK, Polonis VR, Alving CR, Rao M, Rao VB. 2013. Designing a soluble near full-length HIV-1 gp41 trimer. *J Biol Chem* 288:234–246. <https://doi.org/10.1074/jbc.M112.424432>.
17. Yang X, Lee J, Mahony EM, Kwong PD, Wyatt R, Sodroski J. 2002. Highly stable trimers formed by human immunodeficiency virus type 1 envelope glycoproteins fused with the trimeric motif of T4 bacteriophage fibrin. *J Virol* 76:4634–4642. <https://doi.org/10.1128/jvi.76.9.4634-4642.2002>.
18. Lelj-Garolla B, Mauk AG. 2006. Self-association and chaperone activity of Hsp27 are thermally activated. *J Biol Chem* 281:8169–8174. <https://doi.org/10.1074/jbc.M512553200>.
19. Zhu Y, Yu D, Yan H, Chong H, He Y. 2020. Design of potent membrane fusion inhibitors against SARS-CoV-2, an emerging coronavirus with high fusogenic activity. *J Virol* 94:e00635-20. <https://doi.org/10.1128/JVI.00635-20>.
20. Park SB, Irvin P, Hu Z, Khan M, Hu X, Zeng Q, Chen C, Xu M, Leek M, Zang R, Case JB, Zheng W, Ding S, Liang TJ. 2022. Targeting the fusion process of SARS-CoV-2 infection by small molecule inhibitors. *mBio* 13:e0323821. <https://doi.org/10.1128/mbio.03238-21>.
21. Guo L, Bi W, Wang X, Xu W, Yan R, Zhang Y, Zhao K, Li Y, Zhang M, Cai X, Jiang S, Xie Y, Zhou Q, Lu L, Dang B. 2021. Engineered trimeric ACE2 binds viral spike protein and locks it in “Three-up” conformation to potently inhibit SARS-CoV-2 infection. *Cell Res* 31:98–100. <https://doi.org/10.1038/s41422-020-00438-w>.
22. Chou TC. 2006. Theoretical basis, experimental design, and computerized simulation of synergism and antagonism in drug combination studies. *Pharmacol Rev* 58:621–681. <https://doi.org/10.1124/pr.58.3.10>.
23. Chou TC, Talalay P. 1984. Quantitative analysis of dose-effect relationships: the combined effects of multiple drugs or enzyme inhibitors. *Adv Enzyme Regul* 22:27–55. [https://doi.org/10.1016/0065-2571\(84\)90007-4](https://doi.org/10.1016/0065-2571(84)90007-4).
24. Schoof M, Faust B, Saunders RA, Sangwan S, Rezelj V, Hoppe N, Boone M, Billesbolle CB, Puchades C, Azumaya CM, Kratochvil HT, Zimanyi M, Deshpande I, Liang J, Dickinson S, Nguyen HC, Chio CM, Merz G, Thompson MC, Diwanji D, Schaefer K, Anand AA, Dobzinski N, Zha BS, Simoneau CR, Leon K, White KM, Chio US, Gupta M, Jin M, Li F, Liu Y, Zhang K, Bulkley D, Sun M, Smith AM, Rizo AN, Moss F, Brilot AF, Pourmal S, Trenker R, Pospiech T, Gupta S, Barsi-Rhyné B, Belyy V, Barile-Hill AW, Nock S, Liu Y, Krogan NJ, Ralston CY, QCRG Structural Biology Consortium, et al. 2020. An ultrapotent synthetic nanobody neutralizes SARS-CoV-2 by stabilizing inactive Spike. *Science* 370:1473–1479. <https://doi.org/10.1126/science.abe3255>.
25. Rossler A, Riepler L, Bante D, von Laer D, Kimpel J. 2022. SARS-CoV-2 omicron variant neutralization in serum from vaccinated and convalescent persons. *N Engl J Med* 386:698–700. <https://doi.org/10.1056/NEJMc2119236>.
26. Cao Y, Wang J, Jian F, Xiao T, Song W, Yisimayi A, Huang W, Li Q, Wang P, An R, Wang J, Wang Y, Niu X, Yang S, Liang H, Sun H, Li T, Yu Y, Cui Q, Liu S, Yang X, Du S, Zhang Z, Hao X, Shao F, Jin R, Wang X, Xiao J, Wang Y, Xie XS. 2022. Omicron escapes the majority of existing SARS-CoV-2 neutralizing antibodies. *Nature* 602:657–663. <https://doi.org/10.1038/d41586-021-03796-6>.
27. Xia S, Liu M, Wang C, Xu W, Lan Q, Feng S, Qi F, Bao L, Du L, Liu S, Qin C, Sun F, Shi Z, Zhu Y, Jiang S, Lu L. 2020. Inhibition of SARS-CoV-2 (previously 2019-nCoV) infection by a highly potent pan-coronavirus fusion inhibitor targeting its spike protein that harbors a high capacity to mediate membrane fusion. *Cell Res* 30:343–355. <https://doi.org/10.1038/s41422-020-0305-x>.
28. de Vries RD, Schmitz KS, Bovier FT, Predella C, Khao J, Noack D, Haagmans BL, Herfst S, Stearns KN, Drew-Bear J, Biswas S, Rockx B, McGill G, Dorrello NV, Gellman SH, Alabi CA, de Swart RL, Moscona A, Porotto M. 2021. Intranasal fusion inhibitory lipopeptide prevents direct-contact SARS-CoV-2 transmission in ferrets. *Science* 371:1379–1382. <https://doi.org/10.1126/science.abf4896>.
29. Bi W, Xu W, Cheng L, Xue J, Wang Q, Yu F, Xia S, Wang Q, Li G, Qin C, Lu L, Su L, Jiang S. 2019. IgG Fc-binding motif-conjugated HIV-1 fusion inhibitor exhibits improved potency and in vivo half-life: potential application in combination with broad neutralizing antibodies. *PLoS Pathog* 15:e1008082. <https://doi.org/10.1371/journal.ppat.1008082>.
30. Weissenhorn W, Dessen A, Harrison SC, Skehel JJ, Wiley DC. 1997. Atomic structure of the ectodomain from HIV-1 gp41. *Nature* 387:426–430. <https://doi.org/10.1038/387426a0>.